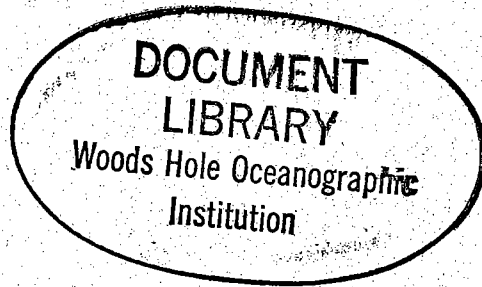
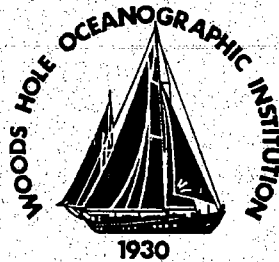


2/25/95
WHOI-95-02

COPY 2



**Woods Hole
Oceanographic
Institution**



Computer Modeling of a Vertical Array in a Stratified Ocean

by

Lin Li

February 1995

Technical Report

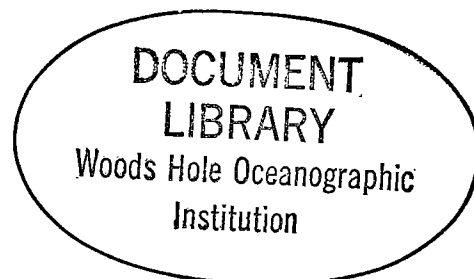
Funding was provided by the National Science Foundation under grant number OCE-91-18943, the Office of Naval Research under grant number N00014-90-J-1493 and the Woods Hole Oceanographic Institution.

Approved for public release; distribution unlimited.

WHOI-95-02

Computer Modeling of a Vertical Array in a Stratified Ocean

by
Lin Li



Woods Hole Oceanographic Institution
Woods Hole, Massachusetts 02543

February 1995

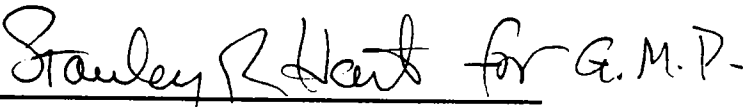
Technical Report

Funding was provided by the National Science Foundation under grant number OCE-91-18943, the Office of Naval Research under grant number N00014-90-J-1493 and the Woods Hole Oceanographic Institution.

Reproduction in whole or in part is permitted for any purpose of the United States Government. This report should be cited as Woods Hole Oceanog. Inst. Tech. Rept., WHOI-95-02.

Approved for public release; distribution unlimited.

Approved for Distribution:



G. Michael Purdy, Chair
Department of Geology and Geophysics



Computer Modeling of a Vertical Array in a Stratified Ocean

by
Lin Li

B. S., B. S., University of Science and Technology of China (1988)

M. S., University of Science and Technology of Beijing (1991)

Submitted in partial fulfillment of the requirements for the degree of

Master of Science

at the

MASSACHUSETTS INSTITUTE OF TECHNOLOGY

and the

WOODS HOLE OCEANOGRAPHIC INSTITUTION

June 1994

© Lin Li 1994

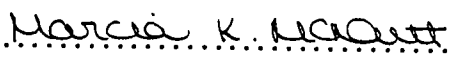
The author hereby grants to MIT and WHOI permission to reproduce and to distribute copies of this thesis document in whole or in part.

Signature of Author 

Joint Program in Oceanography/Applied Ocean Science and Engineering
Massachusetts Institute of Technology
Woods Hole Oceanographic Institution

Certified by ... 

Ralph A. Stephen
Senior Scientist, Woods Hole Oceanographic Institution
Thesis Supervisor

Accepted by 

Marcia K. McNutt
Chair, Joint Committee for Geology and Geophysics
Massachusetts Institute of Technology
Woods Hole Oceanographic Institution
Joint Program in Oceanography/Applied Ocean Science and Engineering

Computer Modeling of a Vertical Array in a Stratified Ocean

by
Lin Li

Submitted to the Massachusetts Institute of Technology/
Woods Hole Oceanographic Institution
Joint Program in Oceanography/Applied Ocean Science and Engineering
on May 6, 1994 in partial fulfillment of the
requirements for the degree of

Master of Science in Oceanography

Abstract

The response of vertical arrays at single frequencies (CW) and for homogeneous media is well known. This paper addresses the issues of frequency dependence and sound velocity gradients for the vertical array response in a deep ocean. I have modified the synthetic seismogram code of Neil Frazer, Subhashis Mallick and Dennis Lindwall to address this problem. The code uses a rearrangement of the Kennett reflectivity algorithm (Kennett, 1974, 1983) which computes the geoacoustic response for depth dependent media and pulse sources by the wave number integration method. The generalized Filon method is applied to the slowness integral for an additional increase in speed (Frazer and Gettrust, 1984; Filon, 1928). The original code computes the response of a single source at a specified depth. The new code has several improvements over the previous one. First, it is a much simplified code addressing only acoustic interaction. The total length is about half the length of the original code. Secondly, the code can compute the response of a vertical array of point sources. By changing the phase delay between the sources, we can steer the beam to the places of most interest. Thirdly, the code reduces considerably numerical noise at large offsets. The original work has numerical noise beyond about 30 km offset at 50 Hz which limits the application of reflectivity modeling in long range problems. The improvement comes with the optimization of the program, both in the speed and program structure. The improved algorithm can be used to get the far offset response (up to 150 km) of a vertical array in the deep ocean at frequencies up to at least 250 Hz. The modeling results are compared to analytical and benchmark solutions. The modified reflectivity code can be applied to the study of pulsed-vertical array sources such as were deployed on the ARSRP (Acoustic Reverberation Special Research Program) acoustic cruises.

Acknowledgments

This work was supported by the National Science Foundation under grant number OCE-91-18943, the Office of Naval Research under grant number N00014-90-J-1493 and Woods Hole Oceanographic Institution.

The successful completion of this thesis was made possible by the support and encouragement of my friends and colleagues. Special appreciation is given to,

- Ralph Stephen, my advisor, for his confidence, great guidance, patience and friendship. He always had time to talk with me and always with a positive attitude.
- Marcia McNutt, for her encouragement, suggestion and a lot of help.
- Dick Von Herzen, for his friendly encouragement, his advice both in science and way of life.
- Bob Detrick, for his help and encouragement.
- John Collins, for his help at the time I needed it most.
- Steve Swift, for his introduction and follow-on help in the project.
- Tom Bolmer, did a tremendous job keeping the computer running with good performance.
- Mom and Dad, who raised me to be tough, to be intelligent, to be anyone that I dream to be.
- Lu Zang, my wife, to whom the thesis is dedicated.

Special thanks also go to Emily Hooft, Javier, Cecily ... for their encouragement and help. Thanks God for giving me the strength and the luck to be with those nice people.

Thesis Supervisor: Ralph Stephen
Senior Scientist
Woods Hole Oceanographic Institution

Contents

1	Introduction	13
2	Background	15
2.1	Reflectivity Method	15
2.2	The Reflectivity Function in a Layered Water Column	17
2.3	Computation of the Slowness Integral	21
3	Theory of Vertical Array Interference for Harmonic Sources	25
3.1	Notation and Example Parameters	25
3.2	Dipole Interference	25
3.2.1	The Field from a Single Source	25
3.2.2	The Field from Two Sources	27
3.3	Multiple Source Interference	31
3.3.1	Analysis Using Complex Numbers	31
3.3.2	Multiple Sources with a Free Surface	38
3.3.3	Multiple Sources under a Free Surface with Phase Delay	39
4	A Study of a Ten Element Vertical Array in a Depth Dependent Ocean	45
4.1	Program Development for a Vertical Array	45
4.2	New Program Flow Chart	46
4.3	Reflectivity Modeling	47
4.3.1	Speed of Sound and Ray Paths in the Ocean	47
4.3.2	Model Description	50

4.3.3	Homogeneous Result	50
4.3.4	Gradient Ocean Result	51
5	Comparison of Modified Reflectivity Results with Benchmark Solutions	67
5.1	Test Problem Solutions	67
5.2	Test Case 1	67
5.3	Test Case 7	68
5.4	Discussion	71
6	Conclusions	74

List of Figures

2-1	Reflection and transmission at a thin layer(From Figure 2.10.2. in Clay and Medwin, 1976)	18
2-2	Reflection from a layered half space(From Figure 2.10.3. in Clay and Medwin, 1976)	20
3-1	The Notation for Multiple Source Interference beneath a Free Surface	26
3-2	Interference Patterns for Two CW Sources without a Free Surface Plotted as Rose Diagrams, with zero phase shift	29
3-3	Interference Patterns for Two CW Sources without a Free Surface Plotted as Intensity versus Angle, with zero phase shift	30
3-4	Interference Patterns for a Ten Element Array without a Free Surface (I), plotted as rose diagrams	34
3-5	Interference Patterns for Ten Sources without a Free Surface (II), plotted as rose diagrams	35
3-6	Ten Element Array without a Free Surface (I), plotted as intensity versus angle	36
3-7	Ten Element Array without a Free Surface (II), plotted as intensity versus angle	37
3-8	Interference Patterns for Ten Element Array with a Free Surface (I), plotted as rose diagrams	40
3-9	Interference Patterns for Ten Element Array with a Free Surface (II), plotted as rose diagrams	41

3-10	Ten Element Array with a Free Surface (I), plotted as intensity versus angle	42
3-11	Ten Element Array with a Free Surface (II), plotted as intensity versus angle	43
4-1	Ray diagram for typical Atlantic Ocean sound channel, depicting channeled rays and refracted-surface-reflected(RSR) rays; sound speed profile is at the right. The angles are grazing angles at the axis of the sound channel. (Ewing and Worzel, 1948.)	48
4-2	The profile of sound speed used in the modeling	49
4-3	The homogeneous ocean response for a 10 element vertical array under a free surface with a 0 degree beam angle. The agreement is good out to 40 km. The solid line is for the reflectivity modeling, the dash-dot line is for theoretical results, the dash line is the theoretical result for the ten element array and also its image (they are the the same). Note that all curves have been normalized to a maximum value of one. . .	53
4-4	The homogeneous ocean response for a 10 element vertical array under a free surface with a 15 degree beam angle. The agreement is good out to 40 km. The solid line is for the reflectivity modeling, the dash-dot line is for theoretical results, the dash line and dots line are the theoretical results for the ten element array and its image respectively. Note that all curves have been normalized to a maximum value of one.	54
4-5	The homogeneous ocean response for a 10 element vertical array under a free surface with a 30 degree beam angle. The agreement is good out to 40 km. The solid line is for the reflectivity modeling, the dash-dot line is for theoretical results, the dash line and dots line are the theoretical results for the ten element array and its image respectively. Note that all curves have been normalized to a maximum value of one.	55

- 4-6 The homogeneous ocean response for a 10 element vertical array under a free surface with a 45 degree beam angle. The agreement is good out to 40 km. The solid line is for the reflectivity modeling, the dash-dot line is for theoretical results, the dash line and dots line are the theoretical results for the ten element array and its image respectively. Note that all curves have been normalized to a maximum value of one. 56
- 4-7 The homogeneous ocean response for a 10 element vertical array under a free surface with a 60 degree beam angle. The agreement is good out to 40 km. The solid line is for the reflectivity modeling, the dash-dot line is for theoretical results, the dash line and dots line are the theoretical results for the ten element array and its image respectively. Note that all curves have been normalized to a maximum value of one. 57
- 4-8 The homogeneous ocean response for a 10 element vertical array under a free surface with a 75 degree beam angle. The agreement is good out to 40 km. The solid line is for the reflectivity modeling, the dash-dot line is for theoretical results, the dash line and dots line are the theoretical results for the ten element array and its image respectively. Note that all curves have been normalized to a maximum value of one. 58
- 4-9 The homogeneous ocean response for a 10 element vertical array under a free surface with a 90 degree beam angle. The agreement is good out to 40 km. The solid line is for the reflectivity modeling, the dash-dot line is for theoretical results, the dash line and dots line are the theoretical results for the ten element array and its image respectively. Note that all curves have been normalized to a maximum value of one. 59

- 4-10 The gradient ocean response for a 10 element vertical array (50 Hz) with a 0 degree beam angle (solid line). The gradient has the effect of increasing the amplitudes between 25 and 30 km by about 6 dB. Because of geometrical spreading the largest response at the seafloor occurs at 8 km from side lobes. The dashed line is the theoretical result for the ten element array and is given as a reference. Note that all curves have been normalized to a maximum value of one and it would be useful to compare reflectivity for both homogeneous and gradient models. 60
- 4-11 The gradient ocean response for a 10 element vertical array (50 Hz) with a 15 degree beam angle (solid line). The gradient has the effect of increasing the amplitudes between 25 and 30 km by about 6 dB. For a homogeneous ocean a 15 degree beam would intersect the seafloor at 15 km. However because of geometrical spreading the largest response at the seafloor occurs at 8 km from side lobes. The dashed line is the same as dash-dot line in the homogeneous ocean response plot and is given as a reference. Note that all curves have been normalized to a maximum value of one and it would be useful to compare reflectivity for both homogeneous and gradient models. 61
- 4-12 The gradient ocean response for a 10 element vertical array (50 Hz) with a 30 degree beam angle (solid line). The gradient has the effect of increasing the amplitudes between 25 and 30 km by about 6 dB. The dashed line is the same as dash-dot line in the homogeneous ocean response plot and is given as a reference. Note that all curves have been normalized to a maximum value of one and it would be useful to compare reflectivity for both homogeneous and gradient models. . . . 62

- 4-13 The gradient ocean response for a 10 element vertical array (50 Hz) with a 45 degree beam angle (solid line). The gradient has the effect of increasing the amplitudes between 25 and 30 km by about 6 dB. The dashed line is the same as dash-dot line in the homogeneous ocean response plot and is given as a reference. Note that all curves have been normalized to a maximum value of one and it would be useful to compare reflectivity for both homogeneous and gradient models. . . . 63
- 4-14 The gradient ocean response for a 10 element vertical array (50 Hz) with a 60 degree beam angle (solid line). The gradient has the effect of increasing the amplitudes between 25 and 30 km by about 6 dB. The dashed line is the same as dash-dot line in the homogeneous ocean response plot and is given as a reference. Note that all curves have been normalized to a maximum value of one and it would be useful to compare reflectivity for both homogeneous and gradient models. . . . 64
- 4-15 The gradient ocean response for a 10 element vertical array (50 Hz) with a 75 degree beam angle (solid line). The gradient has the effect of increasing the amplitudes between 25 and 30 km by about 6 dB. The dashed line is the same as dash-dot line in the homogeneous ocean response plot and is given as a reference. Note that all curves have been normalized to a maximum value of one and it would be useful to compare reflectivity for both homogeneous and gradient models. . . . 65
- 4-16 The gradient ocean response for a 10 element vertical array (50 Hz) with a 90 degree beam angle (solid line). The gradient has the effect of increasing the amplitudes between 25 and 30 km by about 6 dB. The dashed line is the same as dash-dot line in the homogeneous ocean response plot and is given as a reference. Note that all curves have been normalized to a maximum value of one and it would be useful to compare reflectivity for both homogeneous and gradient models. . . . 66

5-1	Comparison of image reference solution (solid line) with reflectivity result(dotted line)	69
5-2	Comparison of normal-mode reference solution (SNAP with solid line) with reflectivity result(dotted line)	70
5-3	Reflectivity Result of 250 Hz Source for Test 7 Velocity Model	73

Chapter 1

Introduction

The ARSRP (Acoustic Reverberation Special Research Program) Reconnaissance Experiment was conducted from 25 July to 19 August 1991, and in 1993 the ARSRP acquired detailed geological and acoustic backscatter data from three sites in the ARSRP corridor in the western North Atlantic. A vertical line array (VLA) of 10 coherent sources was used, and its beam angle can be steered (Elliot, 1991). Specific long term objectives of these efforts are: 1) "to characterize the variations in bottom topography and sub-bottom properties that control the scattering of low frequency acoustic waves", 2) "to develop theoretical and numerical techniques capable of predicting the low frequency acoustic wavefield scattered from geologically realistic models of the bottom/sub-bottom environment", and 3) "to isolate from these scattering models the physical mechanisms which dominate the long-range reverberation from the seafloor."

The challenge for the ARSRP is to analyze the acoustic and geological data and to demonstrate a predictive modeling capability for low angle seafloor backscatter. In order to achieve such a goal, it is important to model the acoustic responses on the seafloor for the VLA. There are several interesting objectives in the numerical modeling: 1) what is the effect of the free surface on the sea floor response, 2) what is the effect of the ocean velocity gradient on the response, 3) how do the above factors affect CW and pulse sources, etc.

Ray theory and parabolic equation methods (Smith and Tappert, 1993) are com-

mon in ocean acoustics to compute the acoustic field. They are compared in Tolstoy et al. (1985). Özlüer (1992) studied the refraction effects on vertical line array beamforming applying a simple ray theory method. She studied the responses from 10 omnidirectional point sources with linear phase tapering equivalent to a steering of 6 deg depression. There are big inaccuracies involved in the results after 30 km horizontal offset.

In order to study the vertical array interference problem more completely and to get a more accurate picture of the interference response in the deep ocean for a wide variety of outgoing beam angles from the vertical array, we use the reflectivity modeling method. The reflectivity method has been widely used to compute synthetic seismograms in layered media. In fact, it has contributed to a better understanding of the earth's structure, both on the continents and beneath the ocean (for example, Braille and Smith (1975), Spudich and Orcutt (1980a, b), and Kempner and Gettrust (1982a,b)).

Its main advantage is its capacity to compute a total solution of the wave field for a given model. A matrix method is generally used to compute the response of the model in frequency-wavenumber space. This includes contributions from all possible generalized rays within the reflecting zone (Kennett 1974, 1983; Kind, 1976). The original reflectivity version of Fuchs and Müller (1971) required the source and receiver to be above the reflecting zone, but the method was subsequently modified by Stephen (1977) to accommodate a receiver buried within the reflecting zone. In practice, there are some disadvantages of the reflectivity method. The main one is the usually long computation time required in the modeling. So, even though there has been extensive study of the theory of the reflectivity method, adequate care must be taken to implement the theory and also to balance the speed and accuracy. This is especially true for our vertical array problem which has multiple sources and which is required to compute long range responses in the deep ocean.

Chapter 2

Background

2.1 Reflectivity Method

The reflectivity method has long been used by seismologists for modeling both land and marine reflection and refraction data. The method, originally proposed by Fuchs and Müller(1971), was extensively modified by Kennett (1974). The calculations are done essentially in two steps:

- A reflectivity function $R(\omega, p)$ is calculated in the frequency-ray parameter (wavenumber) domain. This is performed by layer iteration starting from the free surface down to the deepest interface. In each step of the iteration, all orders of multiple-bounce paths in the layer are included. At the final step, one obtains a reflectivity function that includes all possible ray paths from the source to the receiver.
- The second step involves numerical evaluation of a double integral of the form

$$u(x, t) = \frac{1}{2\pi} \int d\omega \exp(-i\omega t) \times \int dp f(\omega, p) \exp[\sigma g(p)] \quad (2.1)$$

where $\sigma = i\omega x$ and $g(p) = p$.

The integration over frequency ω is usually carried out by a fast Fourier transform (FFT). A complex frequency with a constant imaginary part is used in the integral

to attenuate the wraparound caused by the use of the FFT.

The integrand of the integral over the ray parameter p is highly oscillatory and use of the trapezoidal rule would require a very small step size in p . Use of a generalized Filon method (GFM) (Frazer, 1978; Frazer and Gettrust, 1984) allows one to use a much larger step size in p . The sampling interval δp depends both on frequency and the maximum range needed for the calculation, i.e., long range and high-frequency calculations require a very small step size in p to avoid spatial aliasing.

The background and limitations of the method are described in the two papers of Mallick and Frazer (1987; 1988). We modified their program for our vertical array problem.

The compressional potential of the wave from an explosive point source is

$$\phi_0(r, z, t) = \frac{1}{R} F\left(t - \frac{R}{\alpha_1}\right) \quad (2.2)$$

where $R^2 = r^2 + z^2$. Its Fourier transform can be written in integral form

$$\bar{\phi}_0(r, z, \omega) = \bar{F}(\omega) \int_0^\infty \frac{k}{j\nu_1} J_0(kr) \exp(-j\nu_1 z) dk \quad (2.3)$$

where $\bar{F}(\omega)$ is the Fourier transform of the excitation function $F(t)$, $J_0(kr)$ the Bessel function of the first kind and order zero, j the imaginary unit, k the horizontal wave number, and

$$\nu_1 = (k_{\alpha_1}^2 - k^2)^{\frac{1}{2}} \quad (2.4)$$

is the vertical wave number ($k_{\alpha_1} = \omega/\alpha_1$).

Since we are mainly interested in the application of synthetic seismograms to explosion seismological studies, we can replace the Bessel functions by their asymptotic approximations for large arguments (Fuchs and Müller, 1971), which is good for $kr > 14$ (Corresponding to a source with a frequency of 200 Hz, this approximation is good for ranges down to 16.7m. The synthetic seismograms based on this

approximation will be incorrect at normal incidence) :

$$J_0(x) \approx \sqrt{\frac{2}{\pi x}} \cos\left(x - \frac{\pi}{4}\right) = \frac{1}{\sqrt{2\pi x}} \left\{ \exp\left[j\left(x - \frac{\pi}{4}\right)\right] + \exp\left[-j\left(x - \frac{\pi}{4}\right)\right] \right\} \quad (2.5)$$

$$Y_0(x) \approx \sqrt{\frac{2}{\pi x}} \sin\left(x - \frac{\pi}{4}\right) = \frac{-j}{\sqrt{2\pi x}} \left\{ \exp\left[j\left(x - \frac{\pi}{4}\right)\right] - \exp\left[-j\left(x - \frac{\pi}{4}\right)\right] \right\} \quad (2.6)$$

Where J_0 and Y_0 are Bessel functions of first and second kind respectively and both are of order zero.

The second exponential term in the above equations corresponds to waves propagating in the positive r -direction (away from the source), whereas the first term describes waves traveling in the negative r -direction (towards the source).

2.2 The Reflectivity Function in a Layered Water Column

Fig. 2-1 shows the geometry and notation for the derivation of a layered half space. The pressure reflection and transmission coefficients at the boundary of layers 1 and 2 for a wave incident from above are:

$$\mathfrak{R}_{12}(\theta_1) = \frac{\rho_2 c_2 \cos \theta_1 - \rho_1 c_1 \cos \theta_2}{\rho_2 c_2 \cos \theta_1 + \rho_1 c_1 \cos \theta_2} \quad (2.7)$$

$$\mathfrak{S}_{12}(\theta_1) = \frac{2\rho_2 c_2 \cos \theta_1}{\rho_2 c_2 \cos \theta_1 + \rho_1 c_1 \cos \theta_2} \quad (2.8)$$

with similar expressions for \mathfrak{R}_{23} and \mathfrak{S}_{23} . From Figure 2-1, the total up-traveling signal is the sum of an infinite number of partial transmissions and reflections. Each path within the layer has a phase delay $2k_2 h_2 \cos \theta_2$, where $k_2 \cos \theta_2$ is the vertical component of the wave number in the layer. By letting the incident signal have unit amplitude, the total reflection \mathfrak{R}_{13} is

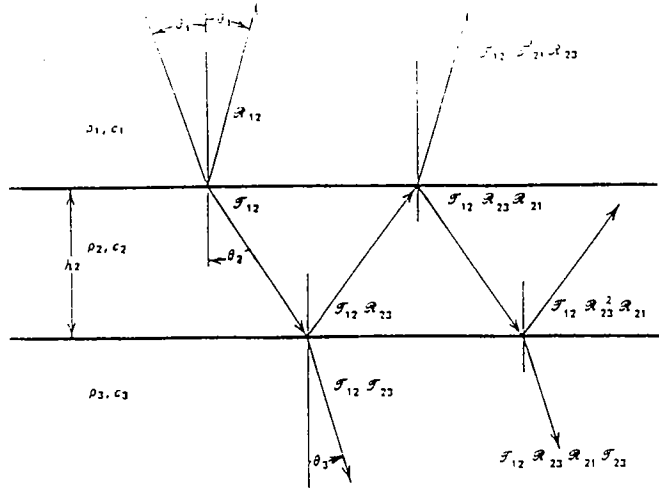


Figure 2-1: Reflection and transmission at a thin layer (From Figure 2.10.2. in Clay and Medwin, 1976)

$$\mathcal{R}_{13}(\theta_1, \omega) = \mathcal{R}_{12} + \mathcal{T}_{12} \mathcal{T}_{21} \mathcal{R}_{23} \exp(-2i\Phi_2) + \mathcal{T}_{12} \mathcal{T}_{21} \mathcal{R}_{23}^2 \mathcal{R}_{21} \exp(-4i\Phi_2) + \dots \quad (2.9)$$

$$\Phi_2 = k_2 h_2 \cos \theta_2 \quad (2.10)$$

After \mathcal{R}_{12} , terms in (2.9) have the form of a geometric series

$$S = \sum_{n=0}^{\infty} r^n = (1 - r)^{-1} \quad \text{for } r < 1$$

$$\mathcal{R}_{13} = \mathcal{R}_{12} + \mathcal{T}_{12} \mathcal{T}_{21} \mathcal{R}_{23} \exp(-2i\Phi_2) \sum_0^{\infty} [\mathcal{R}_{23} \mathcal{R}_{21} \exp(-2i\Phi_2)]^n \quad (2.11)$$

Note that the reflection and transmission coefficients at a single interface are frequency independent (i.e. a function of angle or ray parameter only). When the propagation through a layer is considered (i.e. using Φ_2), the coefficients become frequency dependent.

We can reduce equation 2.11 by using the following relations, which come from equations 2.7 and 2.8,

$$\mathfrak{R}_{12} = -\mathfrak{R}_{21} \quad (2.12)$$

$$\mathfrak{S}_{12}\mathfrak{S}_{21} = 1 - \mathfrak{R}_{12}^2. \quad (2.13)$$

We have

$$\mathfrak{R}_{13} = \frac{\mathfrak{R}_{12} + \mathfrak{R}_{23} \exp(-2i\Phi_2)}{1 + \mathfrak{R}_{12}\mathfrak{R}_{23} \exp(-2i\Phi_2)}. \quad (2.14)$$

The transmission through the layer for a unit incident signal is

$$\mathfrak{S}_{13} = \mathfrak{S}_{12}\mathfrak{S}_{23} \exp(-i\Phi_2) + \mathfrak{S}_{12}\mathfrak{S}_{23}\mathfrak{R}_{23}\mathfrak{R}_{21} \exp(-3i\Phi_2) + \dots \quad (2.15)$$

This is a geometric series, and the sum is

$$\mathfrak{S}_{13} = \frac{\mathfrak{S}_{12}\mathfrak{S}_{23} \exp(-i\Phi_2)}{1 + \mathfrak{R}_{12}\mathfrak{R}_{23} \exp(-2i\Phi_2)} \quad (2.16)$$

Both the \mathfrak{R}_{13} and \mathfrak{S}_{13} are oscillatory functions and depend on $\Phi_2 = k_2 h_2 \cos \theta_2$. They are functions of frequency and angle of incidence for a given layer.

We then can derive the total reflection and transmission of n layers, by repeated applications of the single layer coefficient.

As in Fig. 2-2 the reflection from the lower half space is $\mathfrak{R}_{(n-1)n}$. Applying equation 2.14 the reflection coefficient at the top of the $n - 1$ layer is

$$\mathfrak{R}_{(n-1)n} = \frac{\mathfrak{R}_{(n-2)(n-1)} + \mathfrak{R}_{(n-1)n} \exp(-2i\Phi_{n-1})}{1 + \mathfrak{R}_{(n-2)(n-1)}\mathfrak{R}_{(n-1)n} \exp(-2i\Phi_{n-1})}. \quad (2.17)$$

We can repeat the above process to get $\mathfrak{R}_{(n-3)n}$, the reflection coefficient for the layers beneath the interface, which is

$$\mathfrak{R}_{(n-3)n} = \frac{\mathfrak{R}_{(n-3)(n-2)} + \mathfrak{R}_{(n-2)n} \exp(-2i\Phi_{n-2})}{1 + \mathfrak{R}_{(n-3)(n-2)}\mathfrak{R}_{(n-2)n} \exp(-2i\Phi_{n-2})}. \quad (2.18)$$

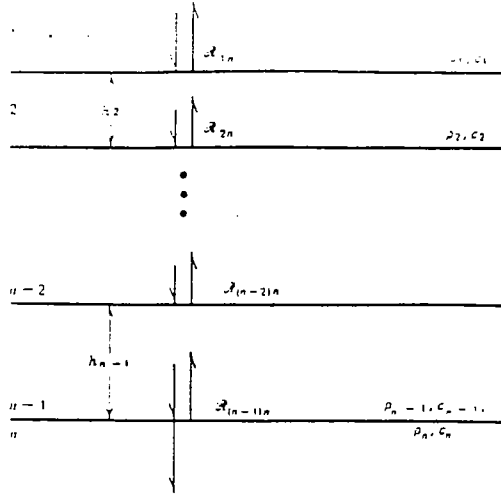


Figure 2-2: Reflection from a layered half space (From Figure 2.10.3. in Clay and Medwin, 1976)

Continuing the above calculation upward to the top, we have

$$\mathfrak{R}_{1n} = \frac{\mathfrak{R}_{12} + \mathfrak{R}_{2n} \exp(-2i\Phi_2)}{1 + \mathfrak{R}_{12}\mathfrak{R}_{2n} \exp(-2i\Phi_2)} \quad (2.19)$$

By letting the reflection coefficient \mathfrak{R}_{1n} represent all the frequency and angle dependence, we simplify the expression for the reflection from a multiple layered half space. The above process can also be applied to get the transmission coefficient from a multiple layered half space. So, for large ranges, we can get the composite pressure reflection and transmission coefficients by applying the above layer iteration approach.

2.3 Computation of the Slowness Integral

In the reflectivity method, we do the numerical evaluation of the slowness integral, in the form

$$u(x, \omega) = \int_0^{\infty} \omega^2 p dp J_0(\omega p x) \tilde{u}(\omega, p) \quad (2.20)$$

where J_0 denotes the first kind Bessel function of order zero. This integral is oscillatory and in a normal integration scheme many steps are necessary in computing this when ωx is large. The step size used is inversely proportional to ωx . The program uses the generalized Filon method given by Frazer (1978) and Frazer and Gettrust (1984), which requires the step size to be inversely proportional to $(\omega x)^{1/2}$, which allows higher ωx response, for a given step size and a given error in computation.

To use the generalized Filon method, we transform the integral of equation 2.20 into (see Chapman 1978)

$$\int_{\Gamma} \frac{\omega^2}{2} p dp H_0^{(1)}(\omega p x) \tilde{u}(\omega, p) \quad (2.21)$$

where Γ is the contour of integration (shown in Fig. 2 of Frazer and Gettrust (1984)). The $H_0^{(1)}$ stands for a Hankel function of type 1 and order zero. The details for the transformation from equation 2.20 to equation 2.21 are shown by Chapman (1978).

We can rewrite equation 2.21 as

$$\int_{\Gamma} f(p) e^{Sg(p)} dp, \quad (2.22)$$

where

$$f(p) = \frac{\omega^2}{2} p H_0^{(1)}(\omega p x) e^{-i\omega p x} \tilde{u}(\omega, p)$$

$$S = i\omega x$$

and

$$g(p) = p$$

Application of the standard trapezoidal rule to the integral in equation 2.22, between the limits a and b , gives the quadrature formula

$$\int_a^b f(p)e^{Sg(p)} dp = \frac{1}{2}[f(a)e^{Sg(a)} + f(b)e^{Sg(b)}]\delta p \quad (2.23)$$

This formula does not work well because it assumes that $f(p)e^{Sg(p)}$ is well approximated by a linear function over the interval (a, b) , while actually it is highly oscillating. If, we assume that both $f(p)$ and $g(p)$ are well approximated by different linear functions on (a, b) , then we get the generalized Filon method analog of the trapezoidal rule (Frazer, 1978):

$$\int_a^b f(p)e^{Sg(p)} dp = \frac{\delta p}{2}[f(a)e^{Sg(a)} + f(b)e^{Sg(b)}], \text{ for } \delta(g) = 0 \quad (2.24)$$

$$\int_a^b f(p)e^{Sg(p)} dp = \frac{\delta p}{S\delta(g)}\left[\delta(fe^{Sg}) - \frac{\delta(f)\delta(e^{Sg})}{S\delta(g)}\right], \text{ otherwise} \quad (2.25)$$

where, δp denotes $p_2 - p_1$, $\delta(g)$ denotes $g(p_2) - g(p_1)$, etc. It can be derived by replacing the integrand in the left-hand side of 2.23 by

$$\left[f_1 + (p - p_1)\frac{\delta(f)}{\delta(p)}\right] \exp\left\{s\left[g_1 + (p - p_1)\frac{\delta(g)}{\delta(p)}\right]\right\}$$

The generalized Filon method greatly improves the quality of the synthetic result. It saves computation time by as much as 80 percent (Mallick and Frazer, 1987). A straightforward error analysis shows that, for a given accuracy, the step size in 2.23 is proportional to $|s|^{-1}$ whereas the step size to 2.25 is proportional to $|s|^{-1/2}$ (Frazer and Gettrust, 1984).

The integral in equation 2.25 is simplified by letting $\delta p = \delta(g)$ and removing the term $\delta p/\delta(g)$:

$$\int_a^b f(p)e^{Sg(p)} dp = \frac{1}{S}\left[\delta(fe^{Sg}) - \frac{\delta(f)\delta(e^{Sg})}{S\delta(g)}\right], \text{ otherwise} \quad (2.26)$$

The results using equation 2.26 show great improvement in terms of the quality of the modeling result. Applying equation 2.25 as in the original program, there is

a big numerical noise problem beyond about 30km offset which limits the application of reflectivity modeling in long range problems. The optimized program using equation 2.26 reduces significantly the noise at large offsets. In the integral 2.25, the p and $g(p)$ are very small. This results in more numerical error than the simplified integral 2.26.

For the reflectivity method, we need to evaluate the integral:

$$u(\omega, x) = \int_0^{\infty - i0} k dk \tilde{u}(\omega, k) J_n(kx) \quad (2.27)$$

in which J_n is the Bessel function of order n , and k is the wavenumber. Here advantage is taken of the relation (Olver, 1972, formula (9.2.19))

$$J_n = M_n \cos \theta_n \quad (2.28)$$

where the definitions of M_n and θ_n are:

$$M_n = \tan^{-1}(Y_n/J_n) \quad (2.29)$$

$$\theta_n = (J_n^2 + Y_n^2)^{\frac{1}{2}} \quad (2.30)$$

The functions M_n and θ_n are available as polynomial approximations (Allen, 1954; Olver, 1972, formula (9.4.3) and (9.4.6)) for values of kx greater than three. For values of kx less than three, exact values of M_n and θ_n could be computed (Olver, 1972, formula (9.2.17)).

The asymptotic expansion of θ_n is (Olver, 1972, formula (9.2.29))

$$\theta_n = kx - \alpha_n + O(|kx|^{-1}) \quad (2.31)$$

where

$$\alpha_n = \frac{1}{4}(2n + 1)\pi$$

So, the equation 2.27 can be written as:

$$u(\omega, x) = \int_0^{\infty-i_0} dk f_1(k) e^{ixk} + \int_0^{\infty-i_0} dk f_2(k) e^{-ixk} \quad (2.32)$$

in which

$$f_1(k) = \frac{1}{2} k \tilde{u}(\omega, k) M_n e^{i(\theta_n - kx)} \quad (2.33)$$

$$f_2(k) = \frac{1}{2} k \tilde{u}(\omega, k) M_n e^{-i(\theta_n - kx)} \quad (2.34)$$

Equation 2.32 is exact, and yet the functions, f_1 and f_2 , are relatively non-oscillatory because of 2.31. More importantly, each integral on the right-hand side of 2.32 is of the form 2.22, and so they can be evaluated using the generalized Filon integration method.

In the modeling of refraction data, x is usually greater than four or five wavelengths, and then the following simpler procedure can be applied. In equation 2.32 replace θ_n by $kx - \alpha_n$ and M_n by $(2/\pi kx)^{1/2}$ (Frazer, 1988).

The $u(\omega, x)$ can now be evaluated using the generalized Filon formula 2.26 with $g(p) = p$ and $s = i\omega x$.

Chapter 3

Theory of Vertical Array

Interference for Harmonic Sources

3.1 Notation and Example Parameters

In our study, we use the following notation as shown in Fig. 3-1. We denote W as the total distance between the top source and the bottom source, d denotes the neighboring source distance, h is the depth of the top source from the free surface and ϕ is the grazing or dip angle of the ray to a receiver at a large distance from the array. Unless otherwise specified, all of the plotting will have the following parameters: $W = 5.49\lambda$, $h = 24.755\lambda$, which implies that the distance between the surface to the midpoint of the 10 sources is 27.5λ and the distance between the neighboring sources is 0.61λ . In the case of a frequency of 250Hz and a velocity of 1.5km/s (so that the wavelength $\lambda = 6\text{m}$), $d = 3.66\text{m}$ and $h + \frac{W}{2} = 165\text{m}$.

3.2 Dipole Interference

3.2.1 The Field from a Single Source

A sinusoidally excited source expands and contracts repeatedly. The resulting contractions (density increases) and dilatations (density decreases) in the medium move

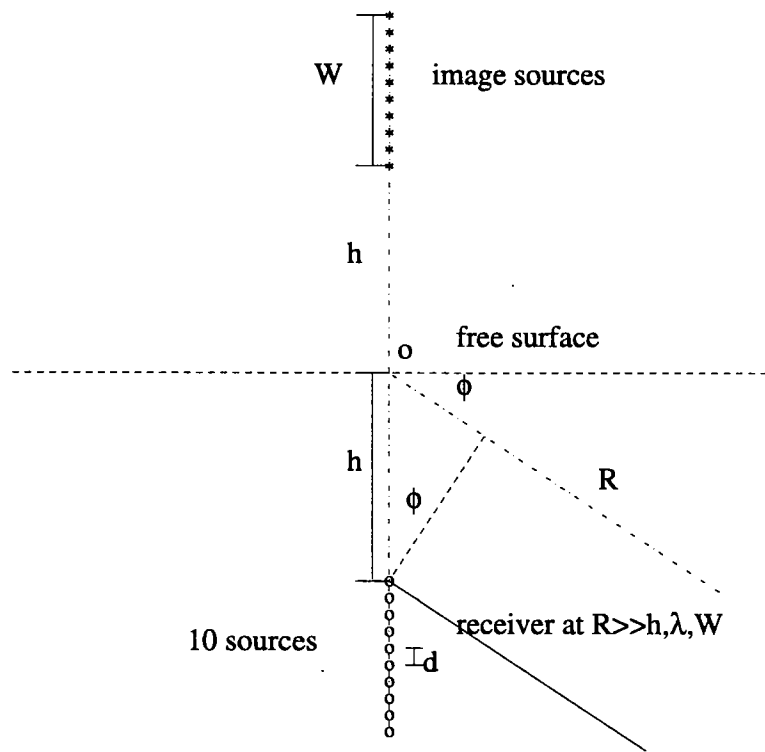


Figure 3-1: The Notation for Multiple Source Interference beneath a Free Surface

away from the source at the sound speed c , as would the disturbance from an impulsive source. This disturbance is called a continuous wave (CW), and it comes from a CW source. The distance between adjacent contractions along the direction of travel is the wavelength λ .

Assume that an omnidirectional CW sinusoidal point source in a homogeneous medium has the pressure at unit distance given by:

$$P = P_0 * \sin(\omega t) \quad (3.1)$$

So, at distance R , the pressure at a given time t will be:

$$P_r = \frac{P_0}{R} * \sin \omega(t - \tau) \quad (3.2)$$

where τ is the phase delay due to the travel time in the medium ($\tau = R/c$) and c is the wave velocity.

The field intensity (transmitted power per unit area), I , will be:

$$I = \frac{\overline{P^2}}{\rho c} = \frac{P_0^2}{2\rho c R^2} \quad (3.3)$$

where $\overline{P^2}$ is the ensemble average of P^2 in the time domain, ρ is the density of the medium and c is the wave speed in the medium.

3.2.2 The Field from Two Sources

Under the same assumption as the single source, two sources will generate an interference pattern.

The pressure at the receiver R is given by

$$P_r = P_1 + P_2 \quad (3.4)$$

where

$$P_1 = \frac{P_0}{R_1} * \sin \phi_1 = \frac{P_0}{R_1} * \sin \omega(t - \tau_1) \quad (3.5)$$

$$P_2 = \frac{P_0}{R_2} * \sin \phi_2 = \frac{P_0}{R_2} * \sin \omega[(t - \tau_2) + \delta_0] \quad (3.6)$$

(τ_1 and τ_2 are the wave travel time from source 1 and source 2 to the receiver respectively, δ_0 is the phase difference of the sources)

Then the field intensity will be:

$$I = \frac{\overline{P^2}}{\rho c} = \frac{\overline{(P_1 + P_2)^2}}{\rho c} = \frac{\overline{P_1^2}}{\rho c} + \frac{\overline{P_2^2}}{\rho c} + \frac{2\overline{P_1 P_2}}{\rho c} = I_1 + I_2 + \frac{2\overline{P_1 P_2}}{\rho c} \quad (3.7)$$

(I_1 and I_2 are the intensity due to single sources in the absence of the other source, and the term $\frac{2\overline{P_1 P_2}}{\rho c}$ corresponds to the interference of the two sources.)

At the same frequency, the phase shift , δ , between waves from two adjacent sources is independent of time:

$$\delta = \phi_2 - \phi_1 = \omega(\tau_1 - \tau_2) + \delta_0 \quad (3.8)$$

$$= \frac{2\pi}{\lambda} * (r_1 - r_2) + \delta_0 \quad (3.9)$$

(λ is wave length, r_1 and r_2 are the distances from the two sources to the receiver respectively, and δ_0 is the phase delay of the top source relative to the bottom source).

Then

$$I = I_1 + I_2 + 2\sqrt{I_1 I_2} \cos \delta \quad (3.10)$$

Discussion:

- When $I_1 = I_2 = I_0$, which is the case when the two sources have the same intensity, we have $I = 4I_0 \cos^2 \frac{\delta}{2}$. For the case with $\delta = 0$, the phase shift offsets the phase difference due to the separation of the sources and we have $I = 4I_0$.
- Figures 3-2 and 3-3 show the interference between two sources at four typical separations of λ , $\lambda/2$, $\lambda/4$ and $\lambda/8$ with ($\delta_0 = 0$). From these plots, it can be seen that within one wavelength, as the distance of the sources decrease,

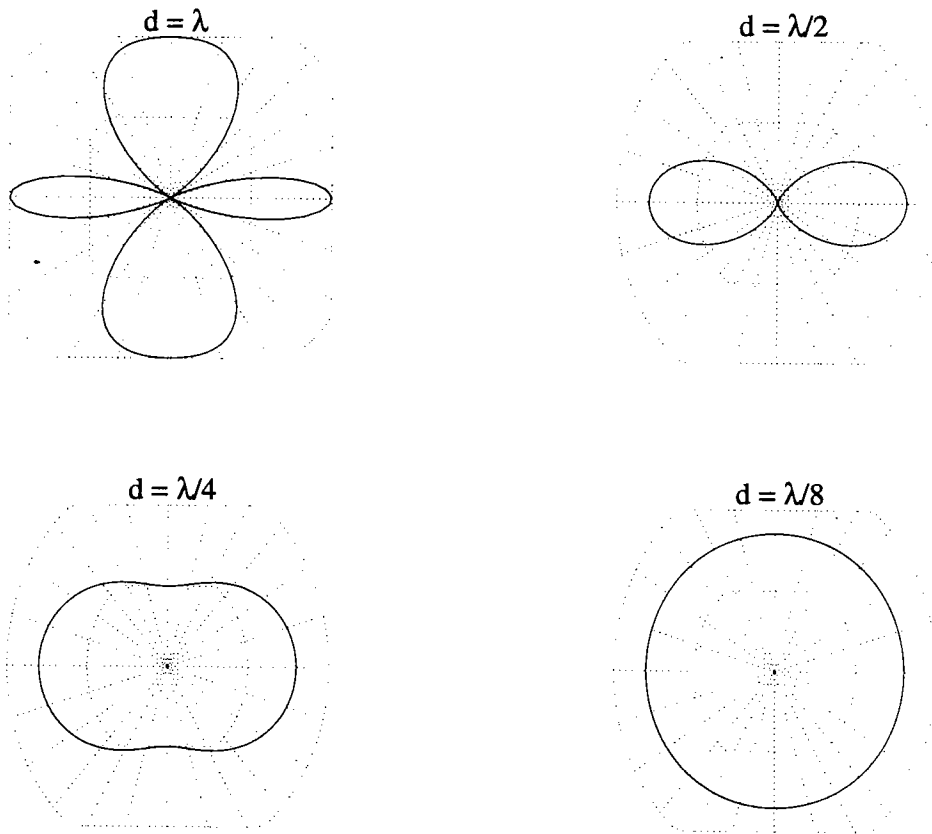


Figure 3-2: Interference Patterns for Two CW Sources without a Free Surface Plotted as Rose Diagrams, with zero phase shift

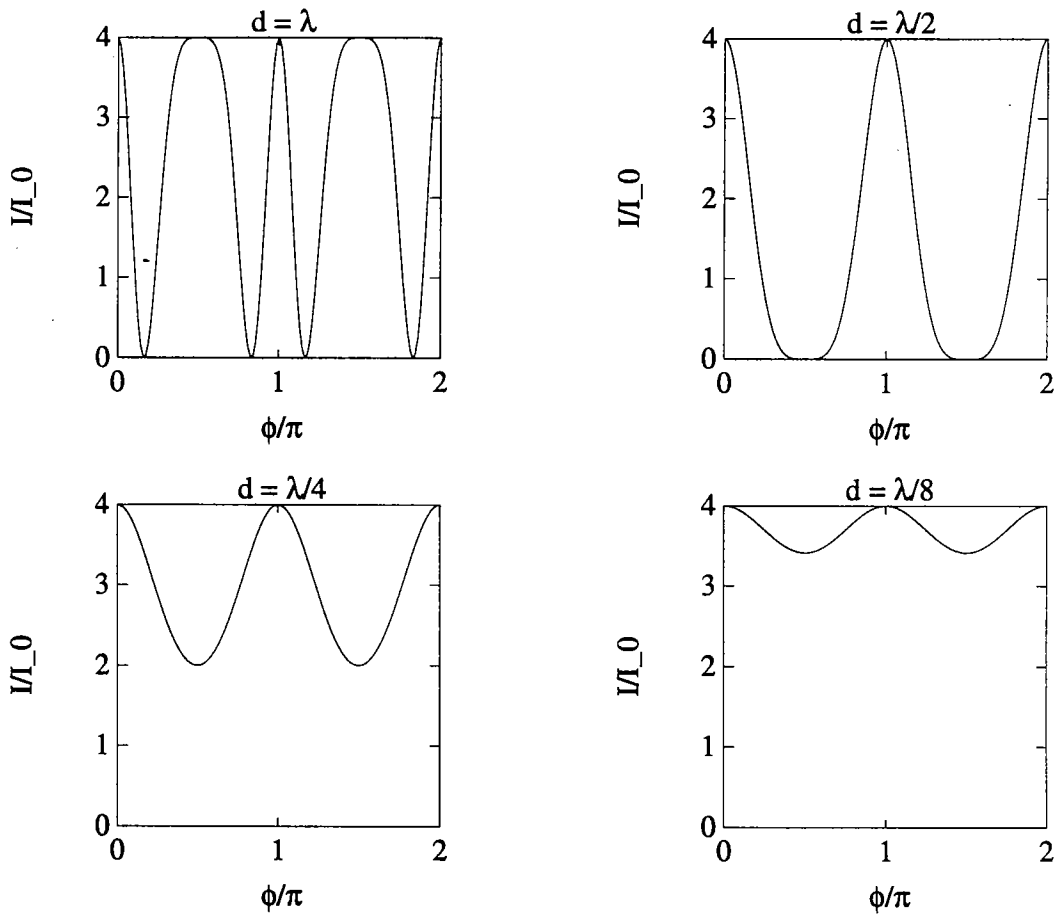


Figure 3-3: Interference Patterns for Two CW Sources without a Free Surface Plotted as Intensity versus Angle, with zero phase shift

the intensity becomes less directionally dependent. All of the plots have the maximum intensity at $\phi = 0$ as they are always 'in phase' in that direction. For the case in which the separation equals one wavelength, the sound is also in phase in the vertical direction and so there is a maximum intensity downwards and upwards. For a half wavelength separation, the sources are exactly out of phase and there is no response at $\phi = 90^\circ$. For the case in which the separation is just an eighth of the wavelength, the intensity pattern is very close to the point source case.

3.3 Multiple Source Interference

3.3.1 Analysis Using Complex Numbers

Complex numbers can simplify the analysis of the interference of multiple sources (see Clay and Medwin, 1976). Many operations involve the sums and differences of angles and the products of trigonometric functions. These operations are simplified by using the relations between trigonometric functions and complex exponential functions.

$$e^{i\Phi} = \cos \Phi + i \sin \Phi \quad (3.11)$$

$$\cos \Phi = \frac{e^{i\Phi} + e^{-i\Phi}}{2}, \sin \Phi = \frac{e^{i\Phi} - e^{-i\Phi}}{2i} \quad (3.12)$$

For N sources evenly spaced over a distance W , the separation of neighboring sources is:

$$d = \frac{W}{N - 1} \quad (3.13)$$

and the pressure fluctuation, $\Delta\rho_n$, of the signal from the n th source, relative to the source at the distance R , is

$$\Delta\rho_n = a \exp\left[i\left(\omega t - kR + \frac{nkW \sin \phi}{N - 1}\right)\right] \quad (3.14)$$

where a is a constant.

So, the pressure fluctuation of n sources is

$$\Delta\rho = a \exp[i(\omega t - kR)] \sum_{n=0}^{N-1} \exp\left(\frac{inkW \sin \phi}{N-1}\right) \quad (3.15)$$

Since $\omega t - kR$ is common to all the signals, we factor it at the beginning and then suppress it by calculating C as follows:

$$\begin{aligned} C &= a \sum_{n=0}^{N-1} \exp\left(\frac{inkW \sin \phi}{N-1}\right) \\ &= a \sum_{n=0}^{N-1} \exp(inkd \sin \phi) \end{aligned}$$

We can show that (see p. 46, Clay and Medwin, 1976):

$$C = Na \left\{ \frac{\exp[iNk(W/2)\frac{\sin \phi}{N-1}]}{\exp[ik(W/2)\frac{\sin \phi}{N-1}]} \right\} \frac{\sin[Nk(W/2)\frac{\sin \phi}{N-1}]}{N \sin[k(W/2)\frac{\sin \phi}{N-1}]} \quad (3.16)$$

The expression in braces has an absolute value of 1 and specifies a phase shift that depends on the choice of origin. The remaining factor is known as the "directional response", D, which is:

$$D = \frac{\sin\left(\frac{N}{N-1} \frac{kW}{2} \sin \phi\right)}{N \sin\left(\frac{1}{N-1} \frac{kW}{2} \sin \phi\right)} \quad (3.17)$$

When N is large, and using

$$\sin[k(W/2)(\sin \phi)/(N-1)] \approx k(W/2)(\sin \phi)/(N-1) \quad (3.18)$$

D becomes

$$D = \frac{\sin \frac{kW \sin \phi}{2}}{\frac{kW \sin \phi}{2}} \quad (3.19)$$

The latter expression has the form $(\sin x)/x$ which has a maximum of one as x tends to zero. This is identical to the directional response of a continuously distributed line source (Clay and Medwin, 1976).